Vortex Flux Channeling in Magnetic Nanoparticle Chains

Martin J. Hÿtch,[1] Rafal E. Dunin-Borkowski,[2,*] Michael R. Scheinfein,[3] Johan Moulin,[4] Cécilie Duhamel,[1] Frédéric Mazaleyrat,[4] and Yannick Champion[1]

[1]*Centre d'Etudes de Chimie Métallurgique, CNRS, 15 rue G. Urbain, 94407 Vitry-sur-Seine, France*
[2]*Department of Materials Science and Metallurgy, University of Cambridge, Pembroke Street, Cambridge CB2 3QZ, United Kingdom*
[3]*Department of Physics, Simon Fraser University, 8888 University Drive, Burnaby, British Columbia, Canada V5A 1S6*
[4]*SATIE-CNRS, Ecole Normale Supérieure de Cachan, 61 avenue du Président Wilson, 94235 Cachan, France*

(Received 7 May 2003; published 18 December 2003)

A detailed understanding of the formation of magnetic vortices in closely spaced ferromagnetic nanoparticles is important for the design of ultra-high-density magnetic devices. Here, we use electron holography and micromagnetic simulations to characterize three-dimensional magnetic vortices in chains of FeNi nanoparticles. We show that the diameters of the vortex cores depend sensitively on their orientation with respect to the chain axis and that vortex formation can be controlled by the presence of smaller particles in the chains.

DOI: 10.1103/PhysRevLett.91.257207 PACS numbers: 75.75.+a, 42.40.Kw

Sophisticated techniques continue to be used to characterize magnetic microstructure in thin films [1], superlattices [2], particle arrays [3–6], and devices [7,8]. Solutions to the Landau-Lifshitz-Gilbert-Langevin (LLGL) equations [9–12] indicate that the measured magnetization states depend sensitively on the initial magnetic state of the system and on interface effects such as those responsible for giant magnetoresistence [13] and delocalized exchange [14,15]. The first direct observation of a magnetic vortex core, in a 55-nm-thick Co film, was made using transmission electron holography and electron diffraction [16]. This measurement provided an upper limit of 15 nm for the core diameter. Recently, spin-polarized scanning tunneling microscopy has been used to show that the diameter of a vortex core in an 8-nm-thick Fe film [17] increased in response to an external field. Here, we apply electron holography and micromagnetic simulations to study *three-dimensional* vortex morphologies in chains of nanocrystals of ferromagnetic $Fe_{0.56}Ni_{0.44}$.

FeNi powders were prepared by cryogenic evaporation-condensation. The molten alloy was held in liquid nitrogen in a levitation furnace. The vapor was condensed rapidly and collected in hexane, where the particles underwent slow oxidation. Alloys with typical grain sizes of 50 nm could be produced [18] in sufficient quantities ($50\ g\,h^{-1}$) for bulk samples [19]. Figure 1(a) shows a chemical map of a representative chain of $Fe_{0.56}Ni_{0.44}$ nanoparticles, which have an average diameter of 50 nm and are coated with 3 nm of oxide. Off-axis electron holograms were acquired at an accelerating voltage of 300 kV using a Philips CM300ST field emission gun transmission electron microscope (TEM) equipped with a ''Lorentz'' lens, a Gatan™ imaging filter, and a 2048 pixel charge-coupled-device camera. The technique [20] involves applying a positive voltage to an electron biprism in order to overlap a coherent electron wave that has passed through the sample with a part of the same electron wave that has passed only through vacuum (Fig. 1(b)). Analysis of the resulting interference pattern allows the phase shift of the electron wave

$$\phi(x) = C_E \int V_0(x,z)dz - \frac{2\pi e}{h} \iint B_\perp(x,z)dxdz \quad (1)$$

to be recovered quantitatively and noninvasively at a spatial resolution close to the nm scale. In Eq. (1), x is a direction in the plane of the sample, z is the electron beam direction, C_E takes a value of $6.53 \times 10^6\ \mathrm{rad\,V^{-1}\,m^{-1}}$ at 300 kV, V_0 is the mean inner potential, and $B_\perp$ is the component of magnetic induction perpendicular to x and z. A representative bright-field

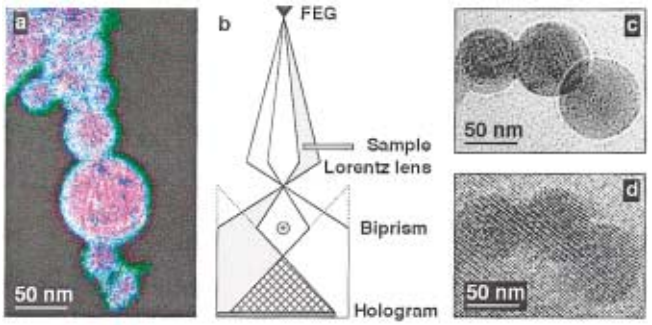

FIG. 1 (color). (a) Chemical map of $Fe_{0.56}Ni_{0.44}$ nanoparticles, obtained using three-window background-subtracted elemental mapping in a Gatan™ imaging filter, showing Fe (red), Ni (blue), and O (green). (b) Ray diagram illustrating the formation of an off-axis electron hologram. (c) Defocused bright-field image and (d) corresponding electron hologram of the end of a chain of $Fe_{0.56}Ni_{0.44}$ particles. Information about the magnetic induction in the sample is encoded in subtle changes in the positions of the holographic interference fringes. The hologram was recorded using an interference fringe spacing of 2.6 nm.

image and a corresponding hologram of part of a chain of $Fe_{0.56}Ni_{0.44}$ particles are shown in Figs. 1(c) and 1(d), respectively. Details about the procedure used to determine the induction in the sample from a hologram are described elsewhere [21]. Although electron holography has been applied to the characterization of chains of magnetic nanoparticles [22–25], vortex states in such chains have never been observed directly.

The magnetization state of an *isolated* particle is traditionally determined by considering the balance between its magnetostatic and exchange energy. The exchange stiffness A of $Fe_{0.56}Ni_{0.44}$ is 1.13 μerg/cm, its saturation magnetization M_S is 1273 emu/cm^3, and the exchange length $l_{ex} = \sqrt{A/2\pi M_S^2}$ is 3.3 nm. $Fe_{0.56}Ni_{0.44}$ particles are therefore expected to be single domain up to a diameter of $\pi l_{ex} = 10$ nm. The presence of an external field (either applied or from dipole-dipole interactions) affects this critical size appreciably. For a material with cubic symmetry, a (classical) multidomain state is expected when the particle size reaches $\sqrt{2}$ times the width of a 90° wall, or ~360 nm for $Fe_{0.56}Ni_{0.44}$. Vortices are therefore expected to form in $Fe_{0.56}Ni_{0.44}$ particles with sizes of 10–360 nm. However, these predictions neglect key factors that influence vortex formation, including interactions between neighboring particles.

Figures 2(a)–2(e) show the magnetic remanent states of five chains of $Fe_{0.56}Ni_{0.44}$ particles, measured using electron holography with the sample in field-free conditions. The magnetization states shown were reproducible when the experiments were repeated several times. The density of the contours, which provide a quantitative measure of the strength and direction of the local flux density, is proportional to the in-plane component of the induction in the sample integrated in the electron beam direction. The unwanted mean inner potential contribution to the phase shift [the first term in Eq. (1)] has been subtracted from each image in Fig. 2 using a procedure described elsewhere [26,27].

The remanent state of a 75 nm $Fe_{0.56}Ni_{0.44}$ particle sandwiched between two smaller (39 and 24 nm) particles is shown in Fig. 2(a). Closely spaced contours run through all three particles in a channel of width 22 ± 4 nm. A comparison of this result with an LLGL simulation (Fig. 3) confirms that the particle contains a vortex, as shown schematically in Fig. 2(f). Whereas the direction of the vortex would depend on the initial conditions for an isolated particle, in a linear chain it depends largely on the relative positions of the particles (and their displacements from the chain axis). The lack of contours on either side of the larger particle results from the induction in these regions being substantially out of plane. The in-plane induction in these regions is also close to zero when integrated along the beam. In Fig. 2(b), a vortex can now be seen end-on in a 71 nm particle at the end of a chain. The particle's neighbors determine the

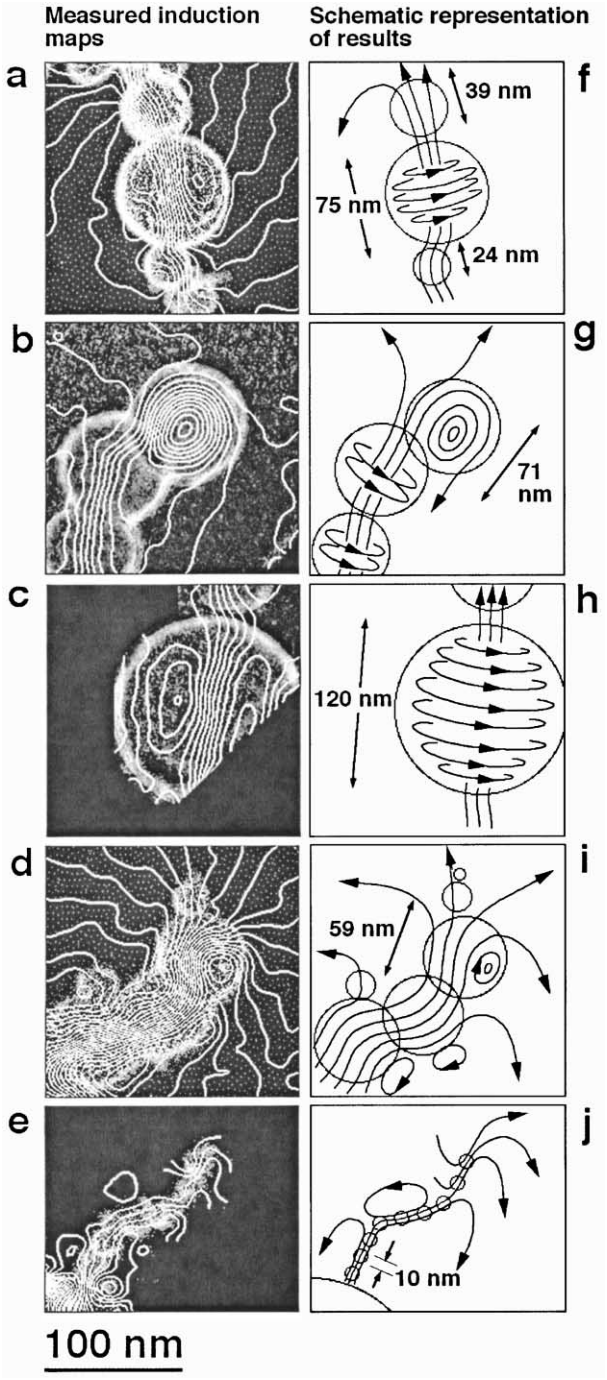

FIG. 2. (a)–(e) Experimental phase contours showing the strength of the local magnetic induction (integrated in the electron beam direction) in five chains of $Fe_{0.56}Ni_{0.44}$ particles, recorded with the electron microscope objective lens switched off. The particle diameters are (a) 75 nm between two smaller particles, (b) 71 nm at the end of a chain, (c) 120 nm, (d) 60 nm, and (e) 10 nm. The contour spacings are 0.083, 0.2, 0.2, 0.167, and 0.05 radians for images (a)–(e), respectively. The mean inner potential contribution to the phase has been removed from each image. (f)–(j) show schematic representations of the magnetic microstructure in the chains. Magnetic vortices spinning about the chain axis are visible in (f)–(h). A vortex spinning perpendicular to the chain axis is also visible in (g).

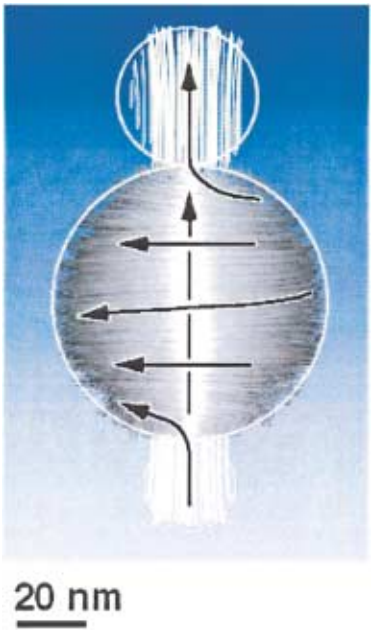

FIG. 3 (color). Streamlines from an LLGL micromagnetic simulation showing the magnetic induction in a 75 nm particle adjacent to 24 and 39 nm particles, illustrating the three-dimensional vector field in the chain of particles shown in Fig. 2(a). The simulation confirms the interpretation shown in Fig. 2(f). The parameters used for the simulation, which was carried out using commercial software [28], were $A = 1.13\ \mu\text{erg/cm}$, $M_s = 1273\ \text{emu/cm}^3$, $K = 0$, $\gamma = 17.6\ \text{MHz/Oe}$, and $\alpha = 1$. The vortex core diameter is identical to the simulated core diameter at the center of a cube given in Fig. 5(a). The phase shift computed from this simulation agreed well with the measured phase shift.

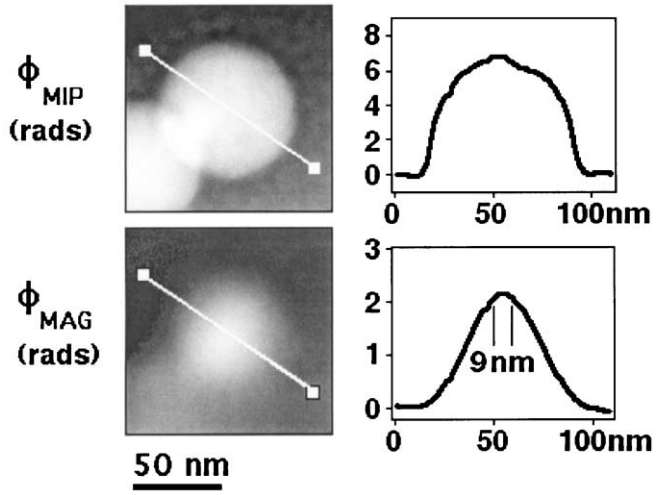

FIG. 4. (a) Mean inner potential ϕ_{MIP} and (b) magnetic ϕ_{MAG} contributions to the measured phase shift for the particle at the end of the chain in Fig. 2(b). The measurement of the vortex core diameter of 9 ± 2 nm from ϕ_{MAG} is not affected by the slight faceting of the particle visible in ϕ_{MIP}.

handedness of the vortex, with the flux channel from the rest of the chain sweeping around the core to form concentric circles [Fig. 2(g)]. The vortex core, which is now perpendicular to the chain axis, is only 9 ± 2 nm in diameter; the larger value in Fig. 2(a) results from dipole-dipole interactions along the chain. Figure 4 shows profiles across the end particle in Fig. 2(b), formed from both the mean inner potential contribution to the measured phase (which is consistent with an almost spherical morphology) and the magnetic contribution to the phase. The departure from a triangular shape in the latter profile is associated with the 9 nm vortex core. In Fig. 2(c), a larger (120 nm) particle appears to possess surface spins of the opposite direction to the core. However, just as in Fig. 2(a), this return flux is associated with the spiral nature of a vortex spinning around a central flux channel [Fig. 2(h)].

LLGL simulations of vortex core diameters in 75 nm $Fe_{0.56}Ni_{0.44}$ cubes are shown in Fig. 5(a). The simulations confirm the observed increase in core diameter when a field is applied parallel to the core. The calculated core diameters for spheres are almost identical to those shown for the centers of cubes in Fig. 5(a); however, the cubes exhibit the additional property that vortices initially perpendicular to the applied field rotate towards the applied field direction above a transverse field of 1300 Oe. Differences between the simulated and measured diameters may result from the use of a uniform field in the calculations, whereas experimentally the dipole-dipole field is localized by neighboring particles in the chain.

In contrast to the observation in Figs. 2(a)–2(c), vortices were never observed in particles below 30 nm in size, while intermediate states were observed in 30–70 nm particles. Holographic phase images from particles with diameters of ~60 and ~10 nm are shown in Figs. 2(d) and 2(e), respectively, with schematic diagrams of the inferred magnetization states shown in Figs. 2(i) and 2(j). In Fig. 2(d), "C" shaped states form along most of the chain, while the end particle contains a distorted vortex with a substantial stray field. In Fig. 2(e), the contours along the chain of 10 nm particles are consistent with the predicted phase shift for single domain particles of this size, which, to our knowledge, are the smallest objects in which magnetization states have been imaged quantitatively at nm spatial resolution.

Our results can be compared with predictions for uniformly magnetized particles by measuring the step in the magnetic contribution to the phase shift across each particle perpendicular to the chain axis. Figure 5(b) shows the theory and measurements, which agree up to a particle size of ~40 nm, above which the measured phase shifts are approximately equal. These results, which are shown as open circles, indicate that the diameters of the observed flux channels are approximately independent of particle size. Calculations based on the magnetostatic energy of a uniformly magnetized sphere [29] suggest

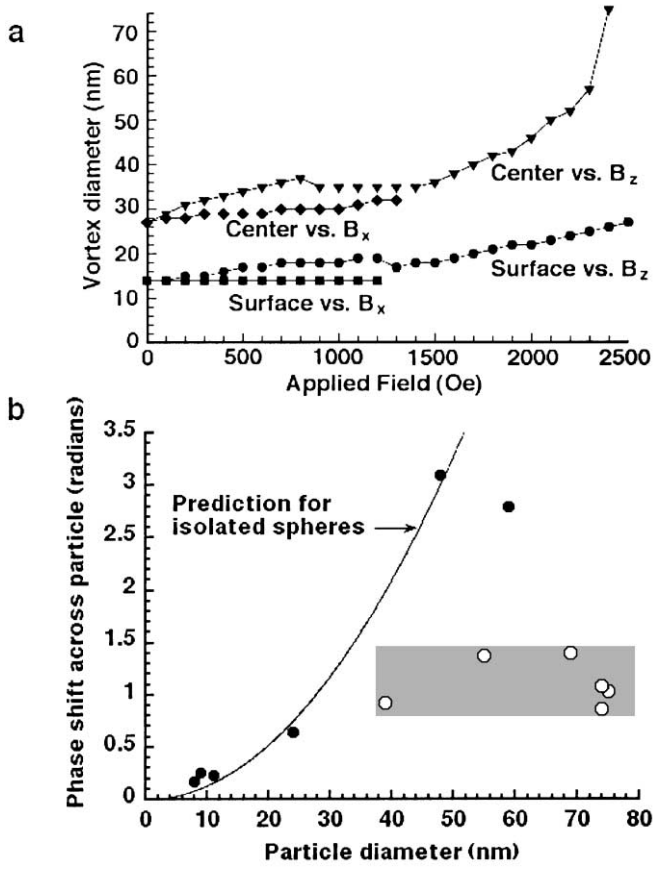

FIG. 5. (a) LLGL simulation of vortex core diameter (defined as the full width at half maximum of the out-of-plane component of the magnetization) at the surface and center of a 75 nm cube of $Fe_{0.56}Ni_{0.44}$ as a function of the externally applied field (along x or z) for a vortex axis along z. The difference between the surface and bulk diameters arises because of the nonuniform demagnetization field. (For spherical particles the core diameter would be more uniform along its length.) (b) Graph showing the predicted phase shift as a function of the diameter of a uniformly magnetized sphere with $M_s = 1273$ emu/cm^3. Experimental results are shown as solid and open circles. The open circles correspond to results from spheres that show flux channeling parallel to the chain axis. Variations in the measurements may be associated with the fact that the chain axes may not lie exactly perpendicular to the electron beam direction.

that such flux channels are possible in spheres whose diameters exceed $4\sqrt{3}l_{\mathrm{ex}} = 24$ nm in $Fe_{0.56}Ni_{0.44}$. An alternative model, in which the spins curl around an easy axis with a null axial component, suggests a critical diameter of 28 nm [30]. Although these calculations agree approximately with our observations, predictions for thin films and isolated spheres are not strictly valid for nanoparticle chains, and the complexity of the observed vortex states highlights the importance of controlling the shapes, sizes, and positions of closely spaced magnetic nanocrystals for applications such as nonvolatile storage devices. These parameters determine the diameters, orientations, and helicities of vortex cores in the particles.

This work was carried out in the framework of the CNRS-funded European Research Group "Quantification and Measurement in Transmission Electron Microscopy." R. D. B. thanks the Royal Society and the E.P.S.R.C. for financial support.

*Corresponding author.
Electronic address: rafal.db@msm.cam.ac.uk

[1] F. Nolting *et al.*, Nature (London) **405**, 767 (2000).
[2] M. Mankos, M. R. Scheinfein, and J. M. Cowley, Adv. Imaging Electron Phys. **98**, 323 (1996).
[3] M. Hehn *et al.*, Science **272**, 1782 (1996).
[4] S. Gider *et al.*, Appl. Phys. Lett. **69**, 3269 (1996).
[5] M. Jamet *et al.*, Phys. Rev. Lett. **86**, 4676 (2001).
[6] A. O. Adeyeye *et al.*, Appl. Phys. Lett. **70**, 1046 (1997).
[7] S. A. Wolf *et al.*, Science **294**, 1488 (2001).
[8] J. C. Slonczewski, J. Magn. Magn. Mater. **159**, L1 (1996).
[9] J. L. Garcia-Palacios and F. J. Lazaro, Phys. Rev. B **58**, 14 937 (1998).
[10] N. Smith, J. Appl. Phys. **90**, 5768 (2001).
[11] G. Brown, M. A. Novotny, and P. A. Rikvold, Phys. Rev. B **64**, 134422 (2001).
[12] S. Kaka and S. E. Russek, Appl. Phys. Lett. **80**, 2958 (2002).
[13] M. N. Baibich *et al.*, Phys. Rev. Lett. **61**, 2472 (1988).
[14] R. Urban *et al.*, Phys. Rev. B **65**, 020402(R) (2001).
[15] Y. Tserkovnyak, A. Brataas, and G. E. W. Bauer, Phys. Rev. Lett. **88**, 117601 (2002).
[16] A. Tonomura, T. Matsuda, J. Endo, T. Arii, and K. Mihama, Phys. Rev. Lett. **44**, 1430 (1980).
[17] A. Wachowiak *et al.*, Science **298**, 577 (2002).
[18] Y. Champion and J. Bigot, Scr. Mater. **35**, 517 (1996).
[19] Y. Champion *et al.*, Science **300**, 310 (2003).
[20] A. Tonomura, Adv. Phys. **41**, 59 (1992).
[21] R. E. Dunin-Borkowski and M. R. McCartney, in *Nanostructured Magnetic Materials*, edited by H. S. Nalwa (American Scientific Publishers, Stevenson Ranch, CA, 2002), pp. 299–325.
[22] R. E. Dunin-Borkowski *et al.*, Science **282**, 1868 (1998).
[23] M. De Graef, N. T. Nuhfer, and M. R. McCartney, J. Microsc. **194**, 84 (1999).
[24] S. Seraphin *et al.*, J. Mater. Res. **14**, 2861 (1999).
[25] S. Signoretti *et al.*, J. Magn. Magn. Mater. **262**, 142 (2003).
[26] R. E. Dunin-Borkowski, M. R. McCartney, D. J. Smith, and S. S. P. Parkin, Ultramicroscopy **74**, 61 (1998).
[27] E. Snoeck *et al.*, Appl. Phys. Lett. **82**, 88 (2003).
[28] Software is available at llgmicro.home.mindspring.com
[29] G. Bertotti, *Hysteresis in Magnetism* (Academic Press, San Diego, 1998).
[30] R. C. O'Handley, *Modern Magnetic Materials* (John Wiley & Sons, New York, 2000).